

High Velocity Clouds, Magnetic Fields, and Foreground Removal

Olivia Walters

Supervisors: Craig Anderson, Naomi McClure-Griffiths

An honours thesis (proposal) submitted for
The Australian National University
Research School of Astronomy and Astrophysics

July 2024

© Olivia Walters 2024

Except where otherwise indicated, this thesis is my own original work.

Olivia Walters
4 July 2024

Acknowledgments

Who do you want to thank?

Abstract

High Velocity Clouds (HVCs) are a proposed solution to how extragalactic gas enters into star-forming galaxies. However, the presence of magnetic fields is required to ensure that HVCs can travel through the halo without being torn apart by ram pressure. This report aims to measure the strength of the magnetic fields present within the Milky Way’s halo and surrounding circumgalactic HVCs, to determine if they can support HVCs as they travel through the Galactic halo. This report uses data from the ASKAP Polarisation Sky Survey of the Universe’s Magnetism (POSSUM) to pull a series of rotation measures (RMs) across the southern sky. These RMs are then converted into magnetic fields using an algorithm, developed using previously collected data from the Smith Cloud. Statistical analysis tools are applied to confirm if hypothesised magnetic fields can support HVCs. The report finds that [Summary of discussion and conclusion] . . .

Contents

Acknowledgments	iii
Abstract	iv
1 Introduction	1
1.1 High Velocity Clouds	1
1.1.1 Chemical Properites and Emission	2
1.2 Magnetic Fields	3
1.2.1 Draping	3
1.2.2 Faraday Rotation	4
1.2.2.1 Noise Interference	5
1.3 Smith Cloud	7
1.4 Report Outline and Objectives	7
2 Data Collection	11
2.1 The Australian Square Kilometer Array Pathfinder (ASKAP)	11
2.2 Observational Data	12
2.2.1 RM Sky Interpolation	12
2.2.2 Other Data Soruces	13
2.3 HVC Selection and Elimination	13
2.4 Data Collation	16
2.4.1 HVC Imaging	16
3 Foreground Subtraction	18
4 Magnetic Field Derivation	19
5 Results	20
6 Discussion	21
7 Conclusions	22
8 Appendix	23
8.1 A - Developed code and data	23
8.2 B - All HVCs	23

List of Figures

1.1	From [Konz et al., 2002], figure 2. An example of a typical HVC shape and structure, specifically that of HVC125+41-207. The contour lines and shading indicate N_{HI} column density.	2
1.2	From [Loi et al., 2019], figure 4. A graph of the relationship between the 1.4 GHz sensitivity of a radio detector array (x-axis) and the minimum number of RM sample points per square degree (y-axis). The black points are not relevant to the report, but the purple line and equation describe the determined relationship.	6
1.3	From [Macquart et al., 2012], figure 1. A graph displaying the effect of observational (stokes parameters) signal-to-noise ratio the resultant faraday depth on a sample set of observations.	8
1.4	From [Lockman et al., 2008], figure 1. A HI image of the Smith Cloud taken from the Green Bank Telescope at a local standard of velocity rest of 100 km s^{-1} . The purpose of the arrows are not meaningful to this paper.	9
2.1	An Aitoff projection of all portions of the RM sky observed by ASKAP for the POSSUM survey. The map is up to date as of May 2024 and all RMs in this map are used in the production of this report. The faraday depth of these RMs are listed in the colourmap.	12
2.2	Cartesian plots of peripheral data maps (left): the HI sky from the Westmeier [2018] modification of the HI4PI survey (top); the H-alpha sky from [Finkbeiner, 2003] (middle); and the Hutschenreuter map from Hutschenreuter and Enßlin [2020]; Hutschenreuter et al. [2022] (bottom). Uncertainty maps for H-alpha and the interpolation are displayed respectively (right). The HI uncertainty is not displayed due to it simply being a scalar multiple of the HI map.	14
2.3	(Left) A graph of all ~ 180000 RMs plotted against their corresponding galactic latitude; (Right) The corresponding graph of all interpolated faraday depths matched to the POSSUM RMs. Both graphs represent a significant level of scatter present in RMs collected near the galactic midplane.	15

2.4	All 15 HVCs used in the analysis of the primary outcome. The HI column density is represented using a greyscale image background. The RMs are represented by circular markers, their size equal to the magnitude and the colour representative of their sign with Red being positive. The black circle is the maximum-extent HVC area and the black 'x' indicates the centre of the HVC.	17
-----	--	----

List of Tables

Introduction

The question of galactic gas accretion is a puzzle that has perplexed Astronomers for decades. Due to the complexities in the structures of star-forming galaxies, there are many factors and potential sources of accretion. What Astronomers do know, at least, is that star-forming galaxies require a continuous supply of fresh gas to continue their star formation.

Due to observational constraints, Astronomers are required to attempt to answer this question by examining the behaviours of our own Milky Way and Local Group environment. This is under the expectation that the Milky Way is typical of a star-forming galaxy.

A major factor to consider when answering this question is where fresh pristine gas comes from, and by what mechanism it takes to enter the disks of star-forming galaxies. The intention of this paper is to continue the examination of one explanation for galactic gas accretion – High Velocity Clouds (HVCs).

1.1 High Velocity Clouds

HVCs are clouds of gas found in the Milky Way's Circumgalactic Medium (CGM) and Galactic Halo and are notable primarily for their high peculiar velocity relative to the Galactic Frame of Rest (GSR), typically $70\text{--}90\text{ km s}^{-1}$ [Wakker, 1991; Wakker and van Woerden, 1997; Blitz et al., 1999]. This increased speed, as will be shown in section 1.2.1, is hypothesized to allow the HVC to survive as it travels through the CGM and halo and reach the Galactic disk and Interstellar Medium (ISM) of the Milky Way.

The origin of HVCs is still unknown, with a few hypotheses as to where they originate. Blitz et al. [1999] suggests that HVCs originate from the Intergalactic Medium (IGM) surrounding the local group. However, there is also a belief that some HVCs likely 'tore off' from satellites like the Magellanic Clouds, due to the presence of their own dark matter subhaloes, and the existence of HVCs in the Magellanic Stream and Leading Arm Kaczmarek et al. [2017]; McClure-Griffiths et al. [2010].

HVCs typically have a neutral mass gas content of $3 \times 10^7 M_{\odot}$ and a dark matter content of $3 \times 10^8 M_{\odot}$. They are generally shaped like comets, with a primary bulb that is approximately $0.5\text{--}25\text{ kpc}$ in diameter - a value that is highly dependent on distance to the Galactic midplane with the lower bound corresponding to approx. 50 kpc and

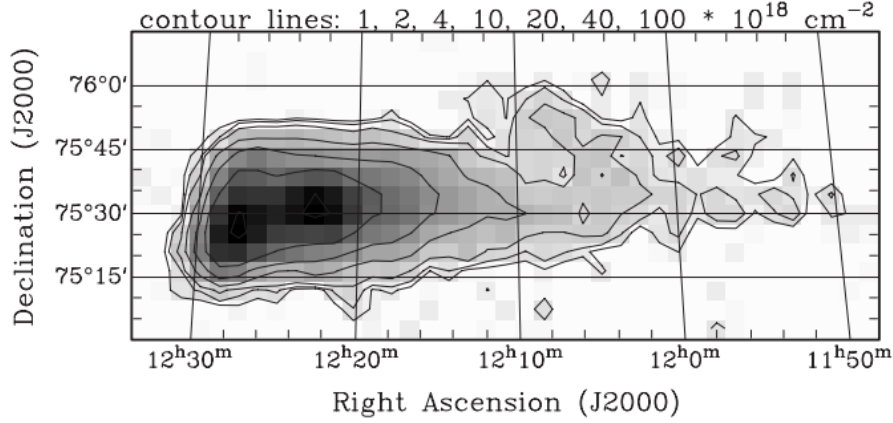


Figure 1.1: From [Konz et al., 2002], figure 2. An example of a typical HVC shape and structure, specifically that of HVC125+41-207. The contour lines and shading indicate N_{HI} column density.

an upper bound of approx. 1 Mpc [Blitz et al., 1999; Konz et al., 2002]. Furthermore, HVCs have tail-like structures that account for one eighth the baryonic mass of the HVC [Konz et al., 2002]. These tails leave behind long streams of gas that remain after collision with the Galactic disk [Putman et al., 2012]. This high distance dependence on size, comet-like structure, and long streaming tails suggest quite conclusively that HVCs shed a lot of material as they make their journey to the ISM.

Figure 1.1 is from [Konz et al., 2002], which provides a typical example of what a HVC looks like in HI, specifically using the example of HVC125+41-207.

1.1.1 Chemical Properties and Emission

HVCs have several characteristics that allow them to be both detected and analysed. Due to their hypothesised extragalactic source, HVCs contain mostly neutral gas such as HI, which can be seen with 21 cm emission [Wakker, 1991; Wakker and van Woerden, 1997; Westmeier, 2018]. HVCs also typically contain molecular gas that emits H-alpha, however due to extinction effects, it is difficult to observe H-alpha emission correctly [Bland-Hawthorn and Maloney, 1999; Finkbeiner, 2003]. Another difficulty for H-alpha analysis is that HVCs typically do not contain CO in significant quantities [Blitz et al., 1999].

Despite HVCs supposed gas purity, there is evidence that HVCs can contain alpha group elements. Hill et al. [2009]; Madsen et al. [2006] found the presence of [NII] 6583Å, [SII] 6716Å, and [OIII] 5007Å emission lines – with a conclusion that Nitrogen abundance is 0.15-0.44 times solar abundance levels. The observation of these emission lines can help constrain the metallicity of any HVC [Hill et al., 2009]. Metallicity is important in both answering the capacity for HVCs to supply fresh gas for star for-

mation, and the mechanism by which HVCs can survive [Grønnow et al., 2018]; more on the latter in section 1.2.1. While HVCs can contain heavier elements Hayakawa and Fukui [2024] finds that these concentrations are low enough that HVCs can remain as viable candidates for fuelling star formation via gas accretion.

HVCs additionally have a temperature relationship. With an average HVC temperature of 10000 K and a range of temperatures ranging from 8000 – 12000 K [Hill et al., 2009; Madsen et al., 2006]. The temperature of a HVC is just around the region in which atomic hydrogen transitions from neutral (HI) to ionised (HII), suggesting that HVCs may be partly ionised [Hill et al., 2009; Madsen et al., 2006; Kawaguchi, 1952]. This temperature relationship is dependent on their position to the Galactic midplane, with HVCs closer to the midplane generally being cooler [Madsen et al., 2006].

1.2 Magnetic Fields

The primary issue facing HVCs as an explanation for gas accretion is its capacity to survive as it travels through the CGM and Galactic halo. As discussed, in section 1.1, HVCs can lose a lot of size and mass as it approaches towards the Galactic disk, with the long trails it leaves behind being evidence for ram-pressure stripping as the HVC collides with the gas present in the halo [Jones et al., 1996; Grønnow et al., 2017, 2022]. Heitsch and Putman [2009] demonstrates that without anything to counter this effect, HVCs with masses under $10^{4.5} M_{\odot}$ would completely disperse within 10 kpc of halo travel.

Additionally, HVCs are subject to Kelvin-Helmholtz (K-H) instabilities, which is triggered by the nature of the HVC being a cloud of warm gas travelling at high speeds through a medium. These K-H instabilities are a significant factor that would lead a to HVCs collapsing before it reaches the Galactic disk [Jones et al., 1996; Grønnow et al., 2017, 2022].

1.2.1 Draping

The proposed solution to handle this problem is magnetic fields. The Galactic halo is magnetised to some degree in a generally turbulent manner [Hill et al., 2010; Han and Qiao, 1994; Jung et al., 2023; Beck et al., 2012]. It is hypothesised that these magnetic fields accumulate the existing magnetic fields and ionised gas in the Galactic halo, causing them to coax the HVC with a shield that protects against ram pressure stripping and suppresses K-H instabilities [Dursi and Pfrommer, 2008; Jones et al., 1996; Konz et al., 2002; Grønnow et al., 2017, 2018; Jung et al., 2022]. This phenomenon is referred to as ‘magnetic draping’.

However, there is not enough evidence to support the magnetic draping hypothe-

sis beyond simulations. As most of the past research, instead, was focused on: technological improvements to surveys [Gaensler et al., 2010; Vanderwoude et al., 2024; Moss et al., 2013; Westmeier, 2018; Taylor et al., 2009; Finkbeiner, 2003; Hutschenreuter and Enßlin, 2020; Hutschenreuter et al., 2022]; the analysis of physical phenomena such as ram pressure stripping [Jones et al., 1996; Grønnow et al., 2017, 2022]; the development of magnetic field derivation techniques [Betti et al., 2019; Grønnow et al., 2017; Hill et al., 2010; Jones et al., 1996; Hill et al., 2013; Schnitzeler, 2010]; and simulations of HVCs [Konz et al., 2002; Grønnow et al., 2017, 2018, 2022; Jung et al., 2022] – all of which lay the groundwork for a proper investigation of magnetic draping.

Previous and recent simulations involve reports produced by Grønnow et al. [2017, 2018, 2022] (henceforth referred to as the “Grønnow simulations”) that provide detailed insight onto how a magnetic draping protects HVCs from collapse, complementing earlier work by Konz et al. [2002]; Jones et al. [1996]. It is shown from the Grønnow simulations that magnetic fields of about 0.3-1 μG can provide stability to HVCs.

However, increasing magnetic field strength beyond a certain threshold can result in more instability; magnetic fields can accelerate the effects of Rayleigh-Taylor (R-T) instabilities and the magnetic pressure applied by the draped fields can also slow down a HVC to the point that it no longer is fast enough to sweep up these magnetic fields. From the Grønnow simulations, the upper threshold where these effects start increasing instability is about 1 μG , thus HVCs should ideally have a “Goldilocks” magnetic field strengths on the order of magnitude of 0.1 μG , with 1 μG being too high, and 0.01 μG being too low.

The effectiveness of magnetic draping is affected by the morphology of these fields and the physical properties of the HVC. The Grønnow simulations state that both the orientation of the magnetic field with respect to the direction of motion of the HVC, and where the magnetic field is located are important considerations. It is expected that not the entire HVC is to be covered in a magnetic field, only the part that is front facing in the direction of travel. While it is possible to draw conclusions about the survivability of a HVC from the strength of the magnetic field, modelling is required to confirm the accuracy of such conclusions [Betti et al., 2019]. The Grønnow simulations also predict that metallicity can affect the HVC’s survivability, with high-density metal-rich clouds and low-density metal-poor clouds being more unstable than their counterparts.

1.2.2 Faraday Rotation

Magnetic fields cannot directly be imaged by a telescope. Instead, researchers can use the phenomenon of Faraday Rotation to quantify the line-of-sight magnetic field strength. Low-frequency polarised radiation tends to rotate as it travels through a medium with a magnetic field present. Thus, by recording the stokes parameters

of incoming light from distant radio sources, one can derive the Rotation Measure (RM) of incoming radiation, which is a statistical quantifier of Faraday Rotation [Vanderwoude et al., 2024; Brentjens and de Bruyn, 2005]. The polarisation angle can be derived from the two orthogonal linear stokes parameters, Q and U, and where ϕ is the polarisation angle:

$$\phi = \frac{1}{2} \arctan \left(\frac{Q}{U} \right) \quad (1.1)$$

Vanderwoude et al. [2024] describes the method by which this report's main source, the Polarisation Sky Survey of the Universe's Magnetism (POSSUM), obtained it's RMs from raw stokes parameters. The value of the RM is derived by establishing a linear relationship between the polarisation angle, $\delta\phi$, and the square of the wavelength of passing radiation, λ , shown in Equation 1.2:

$$\delta\phi = \text{RM}\lambda^2 \quad (1.2)$$

There is a direct connection between RM and line-of-sight magnetic field strength, quantified by the below equation [Betti et al., 2019; Vanderwoude et al., 2024; Hill et al., 2013; Kaczmarek et al., 2017; Hill et al., 2010].

$$\text{RM} = 0.812 \int_{s_{\text{observer}}}^{s_{\text{source}}} \frac{n_e(s)}{\text{cm}^{-2}} \frac{B_{\parallel}}{\mu\text{G pc}} ds \text{ radm}^{-2} \quad (1.3)$$

In which, B_{\parallel} is the magnetic field strength, RM is the Faraday Depth a.k.a. the value of the RM, and n_e is the electron density of the medium as a function of line-of-sight distance s . The analysis of this equation, its solutions, and the use of it in calculating the magnitude of draped magnetic fields is discussed in section 4.

Faraday Rotation also occurs in the ISM, due to the slight magnetisation of the ISM [Ferrière, 2001; Hill et al., 2010; Schnitzeler, 2010]. In addition to this there are many smaller sources of Faraday Rotation that can cause interference with the desired object observations being made. Hence it is also important to remove the foreground from RM observations.

1.2.2.1 Noise Interference

When making radio observations of RMs, a principal factor to consider is signal to noise ratio and detector sensitivity. Radio sources tend to appear in the field after high exposure times, and when they do, they appear as point-like sources. These point-like sources are then collated into an "RM grid" which has a particular density measured in sample points per square degree. The sensitivity of a detector is related to the number of grid points as seen in figure 1.2 [Loi et al., 2019]. At grid densities that are too high, RM sources can bleed into each other, leading to confusion noise. However, no modern radio telescope can reach the confusion limit [Loi et al., 2019].

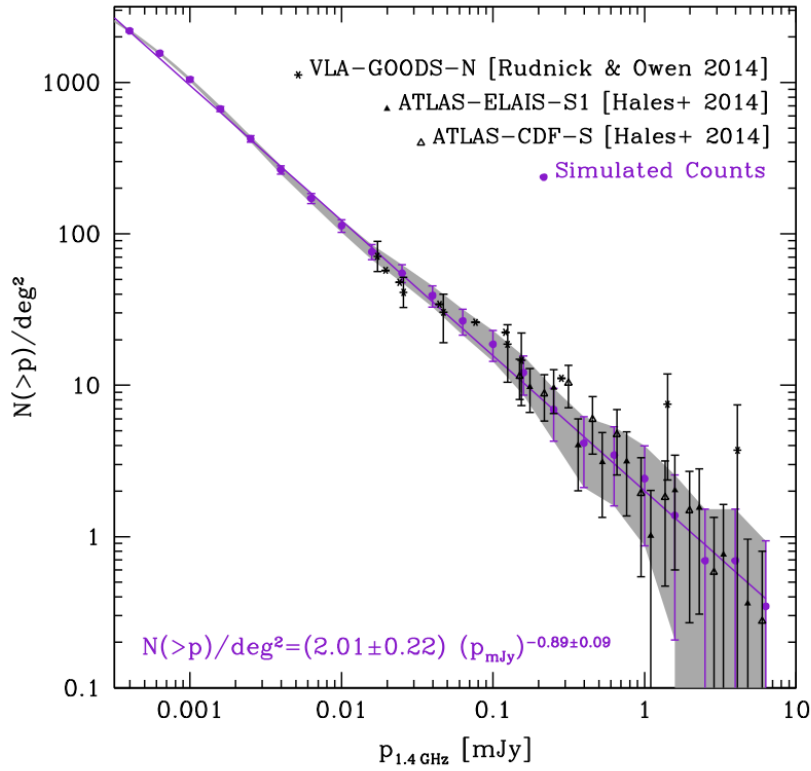


Figure 1.2: From [Loi et al., 2019], figure 4. A graph of the relationship between the 1.4 GHz sensitivity of a radio detector array (x-axis) and the minimum number of RM sample points per square degree (y-axis). The black points are not relevant to the report, but the purple line and equation describe the determined relationship.

Signal to noise is of primary concern when measuring the effect of Faraday Rotation. At low enough signal-to-noise ratios, it is possible to encounter ‘phantom RMs’ which do not accurately represent the real RM [Macquart et al., 2012]. Figure 1.3 gives a visual illustration of this phenomenon. The issue in question is that any observation of RM grids is going to dip below the signal-to-noise threshold of approx. 6, which can introduce an intrinsic scatter in collected RM grid data. There is not much that can be done outside of avoiding regions where the signal-to-noise is likely to be lower (i.e. the Galactic midplane), or to account for it with statistical methods more resistant to large errors.

1.3 Smith Cloud

The Smith Cloud is a large HVC that is in the process of colliding with the Galactic disk [Lockman et al., 2008; Tepper-García and Bland-Hawthorn, 2017; Lockman, 2008]. Unlike most HVCs it is quite large in both mass (at least $10^6 M_{\odot}$ in HI mass) and angular size [Lockman et al., 2008; Tepper-García and Bland-Hawthorn, 2017; Lockman, 2008]. It has a predicted physical size of 3 square kpc, which is large for a HVC close to the Galactic disk [Lockman et al., 2008]. Due to its proximity and size, the Smith Cloud has been used as a source point of analysis for most of the properties already discussed. For example, metallicity tracers and alpha-group elements in Madsen et al. [2006]; Hill et al. [2009] were determined by analysing the Smith Cloud. Figure 1.4 provides an image of the Smith Cloud in HI from Lockman et al. [2008].

The Smith Cloud has additionally already had its magnetic draping effect analysed. Simulations by [Grønnow et al., 2017] and observations by [Hill et al., 2013] both agree on an effective magnetic field of $\sim 8 \mu\text{G}$. Note that this number is well above the Goldilocks zone mentioned in section 1.2.1 – indicating the exceptionality of the Smith Cloud.

While there are other HVCs that have been sampled in the past, the Smith Cloud has been the main source of HVC information. This is a problem, as the Smith Cloud is an outlier amongst most HVCs – evidenced by its unusual size and magnetic field strength, both factors being related. There is a necessity to analyse more typical nearby HVCs to gain an understanding of the effects of magnetic fields.

1.4 Report Outline and Objectives

The primary objective of this report is to (a) construct a rudimentary algorithm for calculating arbitrary HVCs found in the CGM and halo and, (b) use this base algorithm to come up with a *very* rough estimate for the magnetic field strength surrounding typical HVCs. The primary source of data will be POSSUM, which will be used to obtain the primary outcome of the report. Due to the previous lack of robust RM grid

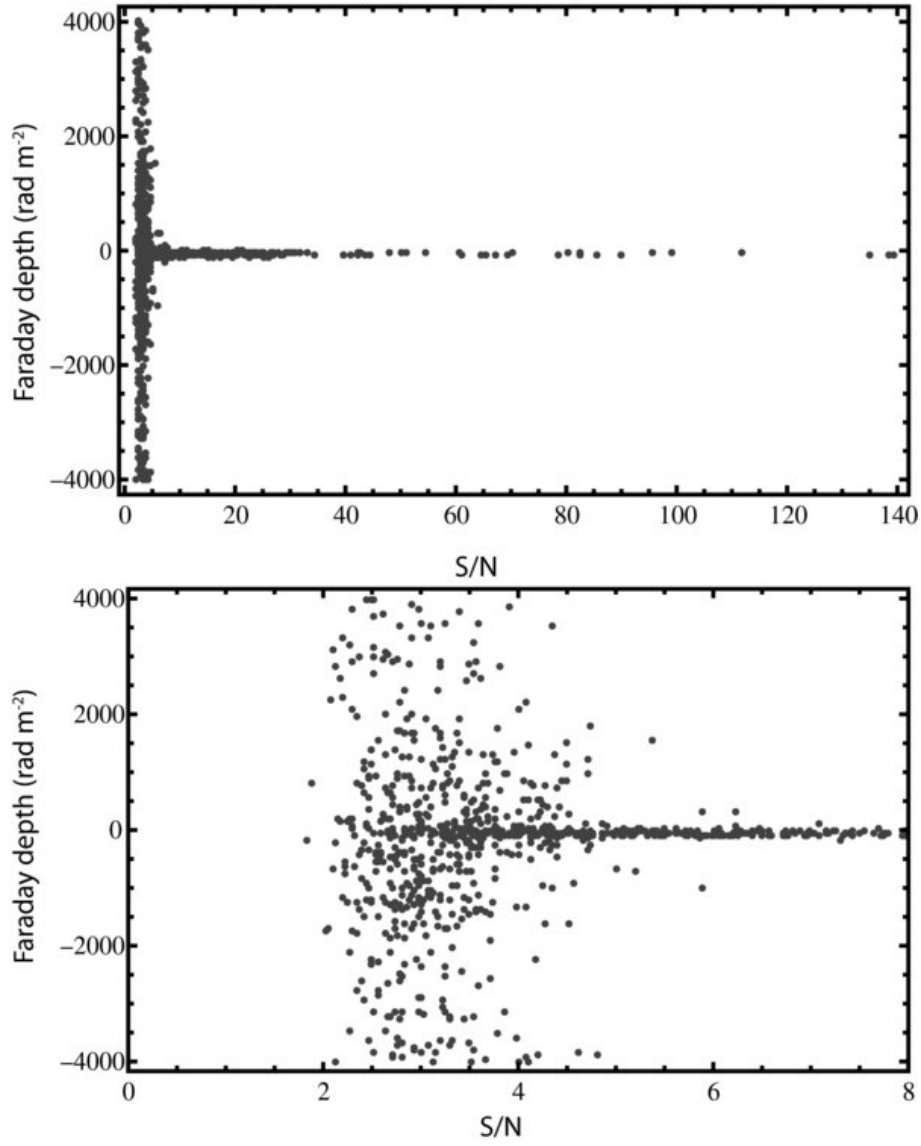


Figure 1.3: From [Macquart et al., 2012], figure 1. A graph displaying the effect of observational (stokes parameters) signal-to-noise ratio the resultant faraday depth on a sample set of observations.

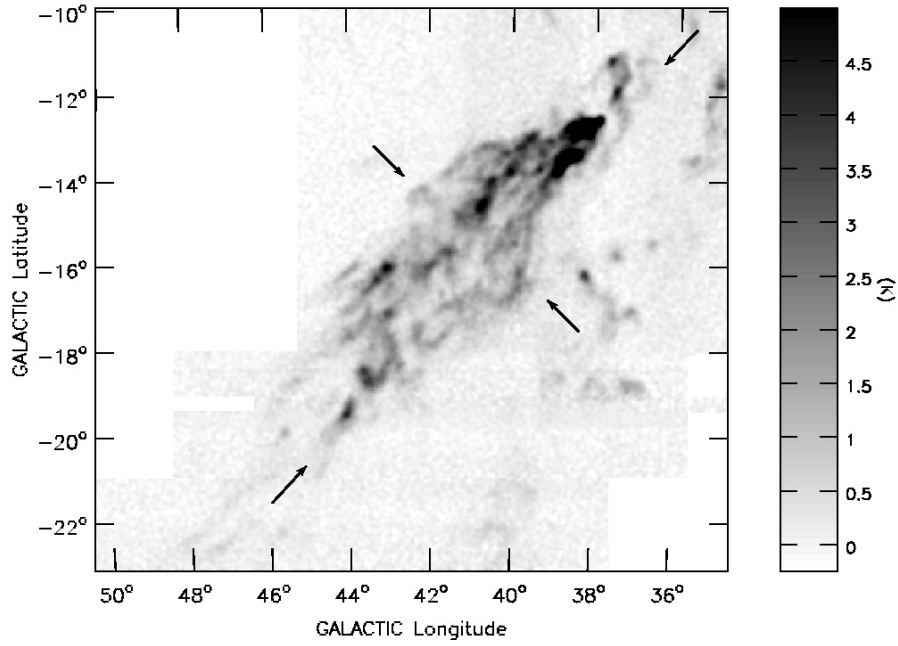


Figure 1.4: From [Lockman et al., 2008], figure 1. A HI image of the Smith Cloud taken from the Green Bank Telescope at a local standard of velocity rest of 100 km s^{-1} . The purpose of the arrows are not meaningful to this paper.

data, along with other periphery data and a large level of required assumptions, it is not possible to come up with an accurate estimate of field strength for any HVC. The best-case scenario is an estimate that is accurate within a single order of magnitude. Hence, why the aim of this report is to lay the foundations for a future, more detailed analysis, of HVCs i.e. it is easier to modify a derivation pipeline than to create one from scratch.

A secondary objective report is integral to completing the primary objective and in future research for all observations of Faraday Rotation: that of foreground removal. Past research, specifically within the analysis of HVCs, has relied on the technique of interpolation to obtain a RM foreground to use in corrections [Schnitzeler, 2010; Moss et al., 2013; Hill et al., 2013]. However, as researchers move onto measurements of magnetism that demand more accuracy, foreground removal needs to equally match that that growing need for accuracy – thus this report also aims to investigate avenues for improving foreground subtraction techniques.

This report is split into eight sections. Section 2 describes the process of how and which data was obtained to achieve the research question, and how this data was collated together. Section 3 summarises the investigation into foreground removal, which is the secondary aim of the research. Section 4 describes how the magnetic fields for HVCs were derived, and the level to which morphology was involved in the analysis. Section 5 provides the results of the scientific investigation and data

analysis. Section 6 discusses the viability of the methods described in the report, along with broader scientific and statistical considerations. Lastly section 7 concludes and outlines the many possible directions for future research. Appendix A (8.1) lists information on how to obtain the program data and algorithms used in research.

Data Collection

To answer both research questions, several sources of data are required. Furthermore, work needs to be done to collate the data together to both measure the magnetic field, quantify the efficacy of foreground removal techniques, and to eliminate problematic data.

2.1 The Australian Square Kilometer Array Pathfinder (ASKAP)

ASKAP represents a recent development in the progress of the field of radio astronomy. It is a part of a new generation of southern-hemisphere telescopes built with the aim to establish the Square-Kilometer Array [Hotan et al., 2021; Gaensler et al., 2010]. ASKAP aims to allow for the progression of research in the “Pre-SKA” era. As mentioned in section 1.4, the importance of preliminary research in the Pre-SKA era is meant to allow for a more efficient process of astronomy in the coming years when the SKA is fully operational. This means that the data and methodology is both rudimentary and advanced compared to previous projects.

POSSUM is an ongoing project using ASKAP with the aim of measuring the RM southern sky. The benefit of using ASKAP as opposed to previous RM sky surveys is the RM grid density ASKAP can provide [Gaensler et al., 2010; Hotan et al., 2021]. Previous surveys such as the NRAO VLA Sky Survey (NVSS) were only able to record an RM grid density of 1 sampling point per square degree, with POSSUM providing a density 30 times greater [Vanderwoude et al., 2024; Gaensler et al., 2010; Hotan et al., 2021; Taylor et al., 2009]. The higher grid density allows for the analysis of regular-sized HVCs in the CGM, as opposed to only the largest HVCs like the Smith Cloud.

Additionally, POSSUM is set to cover a region of the southern sky that has seldom been recorded properly in previous RM grid surveys, primarily due to the lack of RM radio astronomy in the southern sky [Hutschenreuter and Enßlin, 2020; Hutschenreuter et al., 2022; Gaensler et al., 2010]. This allows for the analysis of HVCs which otherwise would not be analysed under legacy data.

Generally, Gaensler et al. [2010] is the reference for current POSSUM data. All POSSUM data is recorded using the ASKAP radio frequency band 1 at 880-1088 MHz

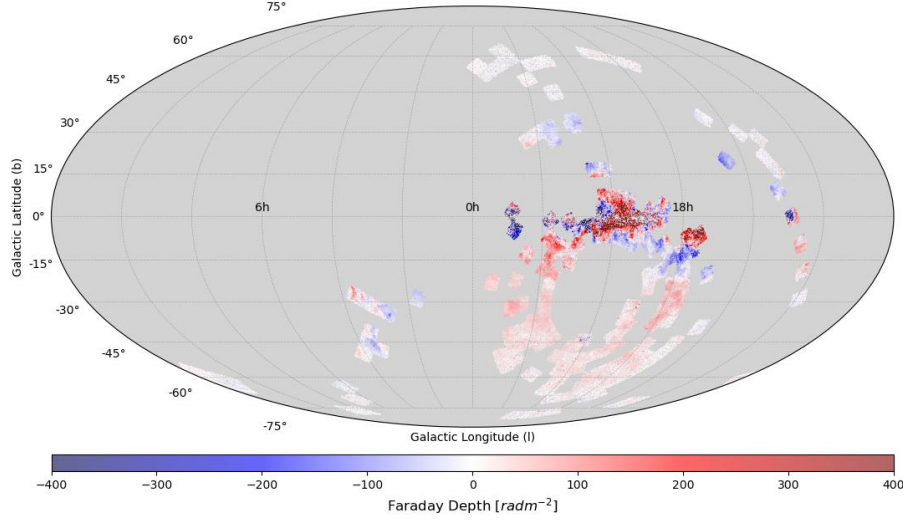


Figure 2.1: An Aitoff projection of all portions of the RM sky observed by ASKAP for the POSSUM survey. The map is up to date as of May 2024 and all RMs in this map are used in the production of this report. The faraday depth of these RMs are listed in the colourmap.

[Vanderwoude et al., 2024; Gaensler et al., 2010]. The POSSUM grid data used in this report was obtained in May 2024, with a total RM source count of 188842. Figure 2.1 represents the entire sample on an Aitoff projection.

2.2 Observational Data

While the primary source of data used was from POSSUM, several other sources of data were employed in the process of analysis.

2.2.1 RM Sky Interpolation

Most important to the process of foreground removal is the interpolation of the RM sky. While more modern research has been done in interpolating the POSSUM data set, for example the recent paper by Khadir et al. [2024], due to POSSUM’s lack of complete sky coverage, it was seen as better to use a whole-sky RM interpolation. The most recent RM sky interpolation came from Hutschenreuter and Enßlin [2020]; Hutschenreuter et al. [2022], which combined all previous sources of RM grid data with free-free emission from the Planck survey. This survey will be referred to as the “Hutschenreuter map” or the “Interpolation” more generally. Most notably, the interpolation has a large ‘blind spot’ near the terrestrial southern pole, with the use of free-free emission to constrain the data better [Hutschenreuter and Enßlin, 2020;

Hutschenreuter et al., 2022]. However, this both points to the necessity of POSSUM in the broad picture, and a potential source of error in the results.

2.2.2 Other Data Sources

Both HI and H-alpha maps were obtained in the process of data collection. While neither were used directly in the calculation of the magnetic field or analysis of foreground removal methods, it was found important to include them in the collated data due to the potential usefulness in future applications of the research. Additionally, HI data were used for the purposes of graphical display in this thesis.

The HI sky was taken from the HI4PI 21 cm survey, with modifications done by Westmeier [2018] to filter for high-velocity HI sources (above a column density of $2 \times 10^{18} \text{cm}^{-2}$). This modification allows for the better resolution of HVCs in the sky, however it eliminates the ability for RMs to directly be analysed using the real HI column density – a factor which will be accounted for in section 4. Unlike all other sources of data, Westmeier [2018] does not provide uncertainties for its HI emissions. It is assumed that the HI uncertainty is approximately equivalent to the Poisson noise i.e. the logarithmic column density is multiplied by one half.

The H-alpha sky was taken from Finkbeiner [2003], which was a collage of three smaller H-alpha surveys. Unfortunately, this map is also limited by the same problems as the Hutschenreuter map, with a notable lack of coverage near the terrestrial south pole. It was decided that the H-alpha map would be included in the process of collation for the purposes of future research potential, even despite the extreme extinction of H-alpha emissions acting as a barrier to proper use in analysis.

Both maps, the Hutschenreuter map, and their respective error maps are displayed in figure 2.2. The only exception being the HI error, which is only altered by a scalar. All data sources collected were first converted to a FITS file under the cartesian projection. Due to the linearity of all RM-specific calculation processes, the use of the cartesian projection will not cause significant or notable distortions in the results.

2.3 HVC Selection and Elimination

All HVC data was obtained from Moss et al. [2013] (hereafter referred to as the “Moss catalogue”) – which was a catalogue of all HVCs found using the Galactic All Sky Survey (GASS). The Moss catalogue is a primary source of data, due to its ability to allow for the location and size analysis of HVCs.

The Moss catalogue includes a total of 1693 HVCs, of which most are not viable candidates for analysis. There are several reasons why a particular HVC in question is not ideal. The first consideration is size. From section 1.1, while HVCs do have incredibly variable sizes, HVCs in the CGM and Halo should generally be of a con-

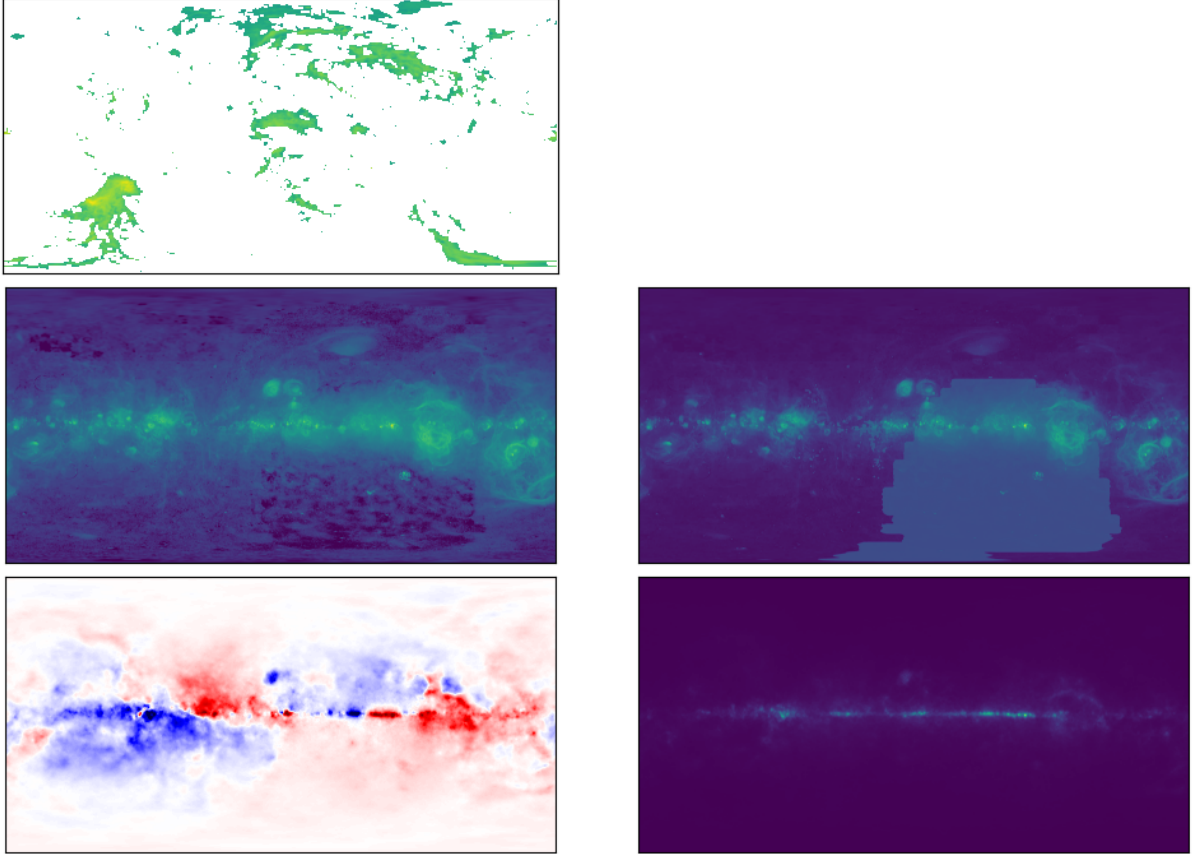


Figure 2.2: Cartesian plots of peripheral data maps (left): the HI sky from the Westmeier [2018] modification of the HI4PI survey (top); the H-alpha sky from [Finkbeiner, 2003] (middle); and the Hutschenreuter map from Hutschenreuter and Enßlin [2020]; Hutschenreuter et al. [2022] (bottom). Uncertainty maps for H-alpha and the interpolation are displayed respectively (right). The HI uncertainty is not displayed due to it simply being a scalar multiple of the HI map.

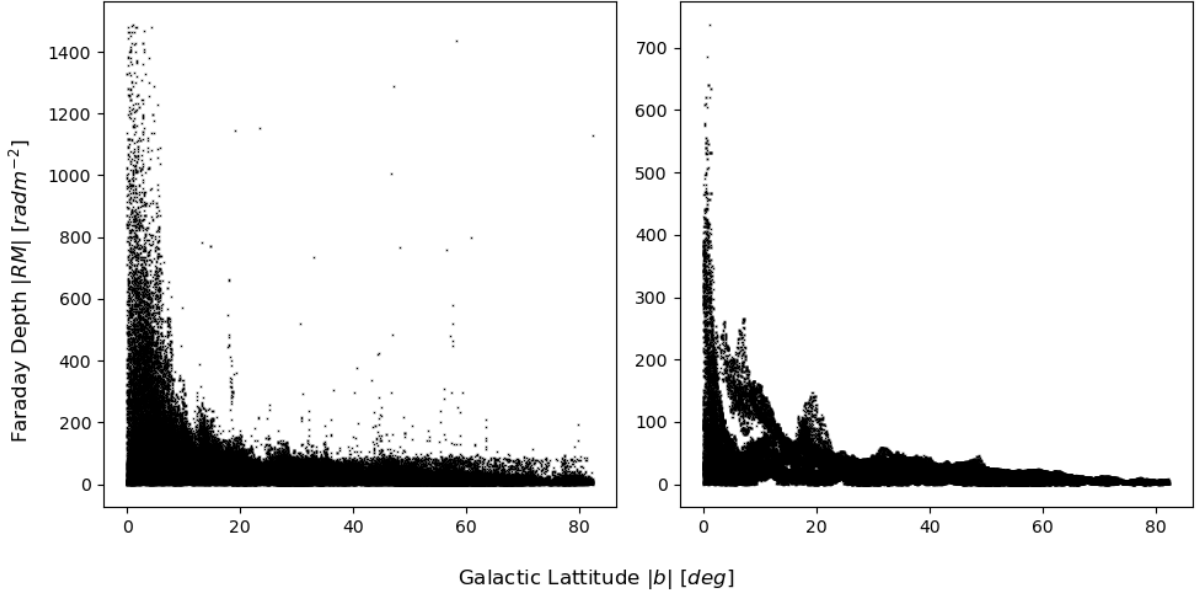


Figure 2.3: (Left) A graph of all ~ 180000 RMs plotted against their corresponding galactic latitude; (Right) The corresponding graph of all interpolated faraday depths matched to the POSSUM RMs. Both graphs represent a significant level of scatter present in RMs collected near the galactic midplane.

sistent size. Exceptions to this rule cannot be included in HVC analysis as they may not be representative of a typical HVC. For example, the Smith Cloud, due to its size, has an abnormally large corresponding magnetic field. Thus, firstly, HVCs that were not in an angular size range of $(1, \pi)$ degrees would be masked out. This reduces the sample to 151 HVCs.

Other considerations made when filtering HVCs were their overlap with the current POSSUM RM grids. Not every HVC is properly covered by the current RM grid. HVCs were filtered out if their centres (obtained from the Moss catalogue) were more than one degree separated from the nearest RM sampling point. This further reduced the sample size to 26 HVCs.

Lastly, there is a major increase in scatter with POSSUM RMs and interpolated RMs closer to the galactic midplane [Schnitzeler, 2010]. This is explored in later sections; however, figure 2.3 represents this scatter. Because of this, HVCs close to the galactic midplane must be eliminated to reduce scatter – specifically HVCs located with Galactic Latitudes $|b| < 20^\circ$ were excluded. This reduces the final sample size to 15.

2.4 Data Collation

Once the data was obtained, calculations were done using the `astropy.wcs` pipeline. For every RM point in the sky, the faraday depth estimated by the interpolation, the HI column density, and the H-alpha flux, including all associated errors were attached to that particular RM sampling point.

2.4.1 HVC Imaging

For each HVC, the HI, H-alpha, interpolation, and RM grid was 'cropped' according to a field twice the size of the maximum HVC source x and y extents. This is to allow for analysis of both RMs in the HVC and surrounding the HVC.

Figure 2.4 presents HI images of all 15 HVCs, the overlapping RM grids, and the cropped HI fields. The filtered Moss catalogue, including all 15 HVCs is displayed in 8.2.

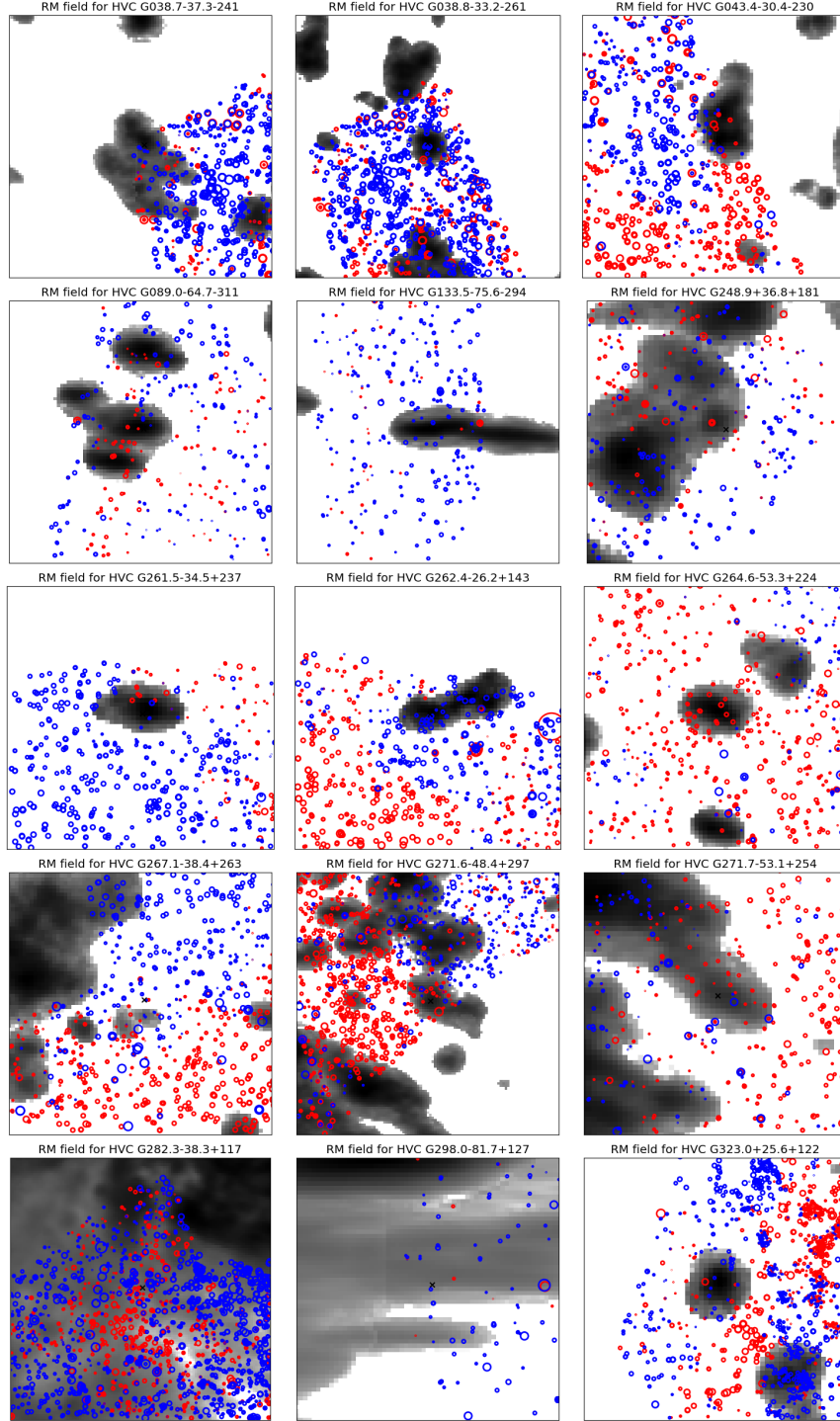


Figure 2.4: All 15 HVCs used in the analysis of the primary outcome. The HI column density is represented using a greyscale image background. The RMs are represented by circular markers, their size equal to the magnitude and the colour representative of their sign with Red being positive. The black circle is the maximum-extent HVC area and the black 'x' indicates the centre of the HVC.

Foreground Subtraction

E

Magnetic Field Derivation

E
Vanderwoude et al. [2024]

Results

Lorem ipsum dolor sit amet, consectetur adipiscing elit. Ut purus elit, vestibulum ut, placerat ac, adipiscing vitae, felis. Curabitur dictum gravida mauris. Nam arcu libero, nonummy eget, consectetur id, vulputate a, magna. Donec vehicula augue eu neque. Pellentesque habitant morbi tristique senectus et netus et malesuada fames ac turpis egestas. Mauris ut leo. Cras viverra metus rhoncus sem. Nulla et lectus vestibulum urna fringilla ultrices. Phasellus eu tellus sit amet tortor gravida placerat. Integer sapien est, iaculis in, pretium quis, viverra ac, nunc. Praesent eget sem vel leo ultrices bibendum. Aenean faucibus. Morbi dolor nulla, malesuada eu, pulvinar at, mollis ac, nulla. Curabitur auctor semper nulla. Donec varius orci eget risus. Duis nibh mi, congue eu, accumsan eleifend, sagittis quis, diam. Duis eget orci sit amet orci dignissim rutrum.

Discussion

Lorem ipsum dolor sit amet, consectetur adipiscing elit. Ut purus elit, vestibulum ut, placerat ac, adipiscing vitae, felis. Curabitur dictum gravida mauris. Nam arcu libero, nonummy eget, consectetur id, vulputate a, magna. Donec vehicula augue eu neque. Pellentesque habitant morbi tristique senectus et netus et malesuada fames ac turpis egestas. Mauris ut leo. Cras viverra metus rhoncus sem. Nulla et lectus vestibulum urna fringilla ultrices. Phasellus eu tellus sit amet tortor gravida placerat. Integer sapien est, iaculis in, pretium quis, viverra ac, nunc. Praesent eget sem vel leo ultrices bibendum. Aenean faucibus. Morbi dolor nulla, malesuada eu, pulvinar at, mollis ac, nulla. Curabitur auctor semper nulla. Donec varius orci eget risus. Duis nibh mi, congue eu, accumsan eleifend, sagittis quis, diam. Duis eget orci sit amet orci dignissim rutrum.

Conclusions

Lorem ipsum dolor sit amet, consectetur adipiscing elit. Ut purus elit, vestibulum ut, placerat ac, adipiscing vitae, felis. Curabitur dictum gravida mauris. Nam arcu libero, nonummy eget, consectetur id, vulputate a, magna. Donec vehicula augue eu neque. Pellentesque habitant morbi tristique senectus et netus et malesuada fames ac turpis egestas. Mauris ut leo. Cras viverra metus rhoncus sem. Nulla et lectus vestibulum urna fringilla ultrices. Phasellus eu tellus sit amet tortor gravida placerat. Integer sapien est, iaculis in, pretium quis, viverra ac, nunc. Praesent eget sem vel leo ultrices bibendum. Aenean faucibus. Morbi dolor nulla, malesuada eu, pulvinar at, mollis ac, nulla. Curabitur auctor semper nulla. Donec varius orci eget risus. Duis nibh mi, congue eu, accumsan eleifend, sagittis quis, diam. Duis eget orci sit amet orci dignissim rutrum.

Appendix

8.1 A - Developed code and data

E

8.2 B - All HVCs

E

Bibliography

- BECK, A. M., LESCH, H., DOLAG, K., KOTARBA, H., GENG, A., AND STASYSZYN, F. A., (2012). Origin of strong magnetic fields in milky way-like galactic haloes. *Monthly Notices of the Royal Astronomical Society*, 422(3), 2152–2163. doi:10.1111/j.1365-2966.2012.20759.x. (cited on page 3)
- BETTI, S. K., HILL, A. S., MAO, S. A., GAENSLER, B. M., LOCKMAN, F. J., MCCLURE-GRIFFITHS, N. M., AND BENJAMIN, R. A., (2019). Constraining the magnetic field of the smith high-velocity cloud using faraday rotation. *The Astrophysical Journal*, 871(2), 215. doi:10.3847/1538-4357/aaf886. (cited on pages 4 and 5)
- BLAND-HAWTHORN, J. AND MALONEY, P. R., (1999). The galactic halo ionizing field and h alpha distances to hvcs. *arXiv*. doi:10.48550/arXiv.astro-ph/9812297. (cited on page 2)
- BLITZ, L., SPERGEL, D. N., TEUBEN, P. J., HARTMANN, D., AND BURTON, W. B., (1999). High-velocity clouds: Building blocks of the local group. *ApJ*, 514(2), 818. doi:10.1086/306963. <https://dx.doi.org/10.1086/306963>. (cited on pages 1 and 2)
- BRENTJENS, M. A. AND DE BRUYN, A. G., (2005). Faraday rotation measure synthesis. *Astronomy & Astrophysics*, 441(3), 1217–1228. doi:10.1051/0004-6361:20052990. (cited on page 5)
- DURSI, L. J. AND PFROMMER, C., (2008). Draping of cluster magnetic fields over bullets and bubbles—morphology and dynamic effects. *The Astrophysical Journal*, 677(2), 993. doi:10.1086/529371. (cited on page 3)
- FERRIÈRE, K. M., (2001). The interstellar environment of our galaxy. *Reviews of Modern Physics*, 73(4), 1031–1066. doi:10.1103/RevModPhys.73.1031. (cited on page 5)
- FINKBEINER, D. P., (2003). A full-sky $h\alpha$ template for microwave foreground prediction. *The Astrophysical Journal*, 146(2), 407. doi:10.1086/374411. (cited on pages vi, 2, 4, 13, and 14)
- GAENSLER, B. M., LANDECKER, T. L., AND TAYLOR, A. R., (2010). Survey science with askap: Polarisation sky survey of the universes’s magnetism (possum). In *Bulletin of the American Astronomical Society*. (cited on pages 4, 11, and 12)

-
- GRÖNNOW, A., TEPPER-GARCÍA, T., AND BLAND-HAWTHORN, J., (2018). Magnetic fields in the galactic halo restrict fountain-driven recycling and accretion. *The Astrophysical Journal*, 865(1), 64. doi:10.3847/1538-4357/aada0e. (cited on pages 3 and 4)
- GRÖNNOW, A., TEPPER-GARCÍA, T., BLAND-HAWTHORN, J., AND FRATERNALI, F., (2022). The role of the halo magnetic field on accretion through high-velocity clouds. *Monthly Notices of the Royal Astronomical Society*, 509(4), 5756–5770. doi:10.1093/mnras/stab3452. (cited on pages 3 and 4)
- GRÖNNOW, A., TEPPER-GARCÍA, T., BLAND-HAWTHORN, J., AND MCCLURE-GRIFFITHS, N. M., (2017). Magnetized high velocity clouds in the galactic halo: A new distance constraint. *The Astrophysical Journal*, 845(1), 69. doi:10.3847/1538-4357/aa7ed2. (cited on pages 3, 4, and 7)
- HAN, J. L. AND QIAO, G. J., (1994). The magnetic field in the disk of our galaxy. *Astronomy & Astrophysics*, 288, 759–772. <https://ui.adsabs.harvard.edu/abs/1994AnA..288..759H>. (cited on page 3)
- HAYAKAWA, T. AND FUKUI, Y., (2024). Dust-to-neutral gas ratio of the intermediate- and high-velocity H I clouds derived based on the sub-mm dust emission for the whole sky. *Monthly Notices of the Royal Astronomical Society*, 529(1), 1–31. doi:10.1093/mnras/stae302. (cited on page 3)
- HEITSCH, F. AND PUTMAN, M. E., (2009). The fate of high-velocity clouds: Warm or cold cosmic rain? *The Astrophysical Journal*, 698(2), 1485. doi:10.1088/0004-637X/698/2/1485. (cited on page 3)
- HILL, A. S., HAFFNER, L. M., AND REYNOLDS, R. J., (2009). Ionized gas in the smith cloud. *The Astrophysical Journal*, 703(2), 1832. doi:10.1088/0004-637X/703/2/1832. (cited on pages 2, 3, and 7)
- HILL, A. S., MAO, S. A., BENJAMIN, R. A., LOCKMAN, F. J., AND MCCLURE-GRIFFITHS, N. M., (2010). A survey of extragalactic faraday rotation at high galactic latitude: The vertical magnetic field of the milky way toward the galactic poles. *The Astrophysical Journal*, 714(2), 1170. doi:10.1088/0004-637X/714/2/1170. (cited on pages 3, 4, and 5)
- HILL, A. S., MAO, S. A., BENJAMIN, R. A., LOCKMAN, F. J., AND MCCLURE-GRIFFITHS, N. M., (2013). Magnetized gas in the smith high velocity cloud. *The Astrophysical Journal*, 777(1), 55. doi:10.1088/0004-637X/777/1/55. (cited on pages 4, 5, 7, and 9)
- HOTAN, A. W., BUNTON, J. D., CHIPPENDALE, A. P., WHITING, M., TUTHILL, J., MOSS, V. A., MCCONNELL, D., AMY, S. W., HUYNH, M. T., ALLISON, J. R., AND ET AL., (2021). Australian square kilometre array pathfinder: I. system description. *Publications of*

- the Astronomical Society of Australia*, 38, e009. doi:10.1017/pasa.2021.1. (cited on page 11)
- HUTSCHENREUTER, S., ANDERSON, C. S., BETTI, S., BOWER, G. C., BROWN, J.-A., BRÜGGEN, M., CARRETTI, E., CLARKE, T., CLEGG, A., COSTA, A., CROFT, S., ECK, C. V., GAENSLER, B. M., DE GASPERIN, F., HAVERKORN, M., HEALD, G., HULL, C. L. H., *, INOUE, M., JOHNSTON-HOLLITT, M., KACZMAREK, J., LAW, C., MA, Y. K., MACMAHON, D., MAO, S. A., RISELEY, C., ROY, S., SHANAHAN, R., SHIMWELL, T., STIL, J., SOBEY, C., O’SULLIVAN, S. P., TASSE, C., VACCA, V., VERNSTROM, T., WILLIAMS, P. K. G., WRIGHT, M., AND ENSSLIN, T. A., (2022). The galactic faraday rotation sky 2020. *Astronomy & Astrophysics*, 657(A43). doi:10.1051/0004-6361/202140486. (cited on pages vi, 4, 11, 12, 13, and 14)
- HUTSCHENREUTER, S. AND ENSSLIN, T. A., (2020). The galactic faraday depth sky revisited. *Astronomy & Astrophysics*, 633(A150). doi:10.1051/0004-6361/201935479. (cited on pages vi, 4, 11, 12, and 14)
- JONES, T. W., RYU, D., AND AND, I. L. T., (1996). The magnetohydrodynamics of supersonic gas clouds: Mhd cosmic bullets and wind-swept clumps. *The Astrophysical Journal*, 473(1), 365. doi:10.1086/178151. (cited on pages 3 and 4)
- JUNG, S. L., GRØNNOW, A., AND MCCLURE-GRIFFITHS, N. M., (2022). Magnetic field draping around clumpy high-velocity clouds in galactic halo. *Monthly Notices of the Royal Astronomical Society*, 522(3), 4161–4180. doi:10.1093/mnras/stad1236. (cited on pages 3 and 4)
- JUNG, S. L., MCCLURE-GRIFFITHS, N. M., PAKMOR, R., MA, Y. K., HILL, A. S., ECK, C. L. V., AND ANDERSON, C. S., (2023). Sampling the faraday rotation sky of tng50: Imprint of the magnetised circumgalactic medium around milky way-like galaxies. Accepted to MNRAS. (cited on page 3)
- KACZMAREK, J. F., PURCELL, C. R., GAENSLER, B. M., MCCLURE-GRIFFITHS, N. M., AND STEVENS, J., (2017). Detection of a coherent magnetic field in the magellanic bridge through faraday rotation. *Monthly Notices of the Royal Astronomical Society*, 467(2), 1776–1794. doi:10.1093/mnras/stx206. (cited on pages 1 and 5)
- KAWAGUCHI, I., (1952). On the excitation and ionization temperature of the hydrogen in the chromosphere. *Publications of the Astronomical Society of Japan*, 4, 131. (cited on page 3)
- KHADIR, A., PANDHI, A., HUTSCHENREUTER, S., GAENSLER, B. M., VANDERWOUDE, S., WEST, J. L., AND O’SULLIVAN, S. P., (2024). Choosing interpolation techniques for reconstructing galactic faraday rotation. Submitted to ApJ. (cited on page 12)

-
- KONZ, C., BRÜNS, C., AND BIRK, G. T., (2002). Dynamical evolution of high velocity clouds in the intergalactic medium. *Astronomy & Astrophysics*, 391(2), 713–723. doi:10.1051/0004-6361:20020863. (cited on pages vi, 2, 3, and 4)
- LOCKMAN, F. J., (2008). *High-Velocity Clouds Merging with the Milky Way*, chap. 53, 239–242. Springer. ISBN 978-1-4020-6932-1. (cited on page 7)
- LOCKMAN, F. J., BENJAMIN, R. A., HEROUX, A. J., AND LANGSTON, G. I., (2008). The smith cloud: A high-velocity cloud colliding with the milky way. *The Astrophysical Journal*, 679(1), L21. doi:10.1086/588838. (cited on pages vi, 7, and 9)
- LOI, F., MURGIA, M., GOVONI, F., VACCA, V., PRANDONI, I., BONAFEDE, A., AND FERETTI, L., (2019). Simulations of the polarized radio sky and predictions on the confusion limit in polarization for future radio surveys. *Monthly Notices of the Royal Astronomical Society*, 485(4), 5285–5293. doi:10.1093/mnras/stz350. <https://doi.org/10.1093/mnras/stz350>. (cited on pages vi, 5, and 6)
- MACQUART, J.-P., EKERS, R. D., FEAIN, I., AND JOHNSTON-HOLLITT, M., (2012). On the reliability of polarization estimation using rotation measure synthesis. *The Astrophysical Journal*, 750(2), 139. doi:10.1088/0004-637X/750/2/139. <https://dx.doi.org/10.1088/0004-637X/750/2/139>. (cited on pages vi, 7, and 8)
- MADSEN, G. J., REYNOLDS, R. J., AND HAFFNER, L. M., (2006). A multiwavelength optical emission line survey of warm ionized gas in the galaxy. *The Astrophysical Journal*, 652(1), 401. doi:10.1086/508441. (cited on pages 2, 3, and 7)
- MCCLURE-GRIFFITHS, N. M., MADSEN, G. J., GAENSLER, B. M., MCCONNELL, D., AND SCHNITZELER, D. H. F. M., (2010). Measurement of a magnetic field in a leading arm high-velocity cloud. *The Astrophysical Journal*, 725(1), 275. doi:10.1088/0004-637X/725/1/275. (cited on page 1)
- MOSS, V. A., MCCLURE-GRIFFITHS, N. M., MURPHY, T., PISANO, D. J., KUMMERFELD, J. K., AND CURRAN, J. R., (2013). High-velocity clouds in the galactic all sky survey. i. catalog. *The Astrophysical Journal*, 209(1), 12. doi:10.1088/0067-0049/209/1/12. (cited on pages 4, 9, and 13)
- PUTMAN, M., PEEK, J., AND JOUNG, M., (2012). Gaseous galaxy halos. *Annual Reviews of Astronomy & Astrophysics*, 50, 491–529. doi:10.1146/annurev-astro-081811-125612. (cited on page 2)
- SCHNITZELER, D. H. F. M., (2010). The latitude dependence of the rotation measures of nvss sources. *Monthly Notices of the Royal Astronomical Society: Letters*, 409(1), L99–L103. doi:10.48550/arXiv.1011.0737. (cited on pages 4, 5, 9, and 15)

-
- TAYLOR, A. R., STIL, J. M., AND SUNSTRUM, C., (2009). A rotation measure image of the sky. *The Astrophysical Journal*, 702(2), 1230. doi:10.1088/0004-637X/702/2/1230. (cited on pages 4 and 11)
- TEPPER-GARCÍA, T. AND BLAND-HAWTHORN, J., (2017). The Smith Cloud: surviving a high-speed transit of the Galactic disc. *Monthly Notices of the Royal Astronomical Society*, 473(4), 5514–5531. doi:10.1093/mnras/stx2680. <https://doi.org/10.1093/mnras/stx2680>. (cited on page 7)
- VANDERWOUDE, S., WEST, J. L., GAENSLER, B. M., RUDNICK, L., VANECK, C. L., THOMSON, A. J. M., H. ANDERNACH, ANDERSON, C. S., CARRETTI, E., HEALD, G. H., LEAHY, J. P., McCLURE-GRIFFITHS, N. M., O’SULLIVAN, S. P., TAHANI, M., AND WILLIS, A. G., (2024). Prototype faraday rotation measure catalogs from the polarization sky survey of the universe’s magnetism (possum) pilot observations. Submitted to ApJ. (cited on pages 4, 5, 11, 12, and 19)
- WAKKER, B., (1991). High-velocity clouds. *Symposium - International Astronomical Union*, 144, 27–40. doi:10.1017/S0074180900088884. (cited on pages 1 and 2)
- WAKKER, B. P. AND VAN WOERDEN, H., (1997). High-velocity clouds. *Annual Reviews of Astronomy & Astrophysics*, 35, 217–266. doi:10.1146/annurev.astro.35.1.217. (cited on pages 1 and 2)
- WESTMEIER, T., (2018). A new all-sky map of galactic high-velocity clouds from the 21-cm hi4pi survey. *Monthly Notices of the Royal Astronomical Society*, 474(1), 289–299. doi:10.1093/mnras/stx2757. (cited on pages vi, 2, 4, 13, and 14)